

Production of hyperon resonances induced by kaon on a deuteron target

J. Yamagata-Sekihara^{1,*}, T. Sekihara¹, and D. Jido^{2,3}

¹*Institute of Particle and Nuclear Studies, High Energy Accelerator Research Organization (KEK), 1-1, Oho, Ibaraki 305-0801, Japan*

²*Yukawa Institute for Theoretical Physics, Kyoto University, Kyoto 606-8502, Japan*

³*J-PARC Branch, KEK Theory Center, Institute of Particle and Nuclear Studies, High Energy Accelerator Research Organization (KEK), 203-1, Shirakata, Tokai, Ibaraki, 319-1106, Japan*

*E-mail: yamajun@post.kek.jp

.....
The $K^-d \rightarrow \pi Y N$ reaction is theoretically studied so as to investigate the K^- -induced production of the hyperon resonances $\Sigma(1385)$ and $\Lambda(1405)$. For this purpose we take into account the p -wave amplitudes for the meson-baryon two-body scatterings as well as the s -wave amplitudes. Due to the fact that the hyperon resonances are selectively produced from the $\bar{K}N$ channel in this reaction, the $\Lambda(1405)$ peak appears at 1420 MeV, which implies that $\Lambda(1405)$ and $\Sigma(1385)$ could be separately seen in the missing mass spectrum of the emitted nucleon in the $K^-d \rightarrow nX$ reaction. The πY invariant mass spectrum in this study is consistent with experimental data both for $\Sigma(1385)$ and $\Lambda(1405)$. The pion exchange contributions are also included and are found to give smooth background without distorting the peak structure of the hyperon resonances.

1. Introduction

Properties of hyperon resonances are important to understand role of strangeness in hadron physics. Especially, understanding of hyperon resonances located below the $\bar{K}N$ threshold, such as $\Lambda(1405)$ and $\Sigma(1385)$, is essential for physics of strangeness in nuclear matter and nuclei. In addition, because baryonic resonances decay into mesons and a baryon in strong interactions, one can learn basic interactions between hadrons with strangeness from the properties of hyperon resonances.

Among the various hyperon resonances, recent attention is particularly focused on the $\Lambda(1405)$ hyperon resonance with $J^P = 1/2^-$ and $I = 0$. The $\Lambda(1405)$ resonance has been considered for long time as a quasibound state of $\bar{K}N$ [1], being extremely important resonance to understand $\bar{K}N$ interaction. Theoretically, $\Lambda(1405)$ is successfully reproduced as dynamically generated states in coupled-channels approach based on chiral dynamics [2–13], and this approach has confirmed that the $\Lambda(1405)$ is predominantly described by meson-baryon components [14]. Recently it has been also pointed out in Ref. [8] that the $\Lambda(1405)$ is composed by two resonance states having different coupling nature and that the one which dominantly couples to the $\bar{K}N$ channel is located at 1420 MeV instead of nominal 1405 MeV. Since the resonance position of the $\Lambda(1405)$ in the $\bar{K}N$ channel is strongly related to the strength of the $\bar{K}N$ interaction, it is very important to observe $\Lambda(1405)$ spectra in the $\bar{K}N \rightarrow \pi\Sigma$ channel and pin down the resonance position of the $\Lambda(1405)$ seen below the $\bar{K}N$ threshold.

Several ideas to observe the $\Lambda(1405)$ initiated by the $\bar{K}N$ channel have been proposed in Refs. [8, 15–22]. One of the promising ways to form the $\Lambda(1405)$ in the $\bar{K}N$ channel is to use nuclear reactions with K^- beam, such as in-flight $K^-d \rightarrow \Lambda(1405)n$, as discussed in Refs. [19, 20], in which Fermi motion of nucleon and \bar{K} multi-scattering with nucleons help to create $\Lambda(1405)$ by $\bar{K}N$ below its threshold. In Ref. [19] it has been found that, in the $K^-d \rightarrow \Lambda(1405)n$ reaction with intermediate K^- beam energy, $\Lambda(1405)$ production dominantly takes place in double scattering process, in which the incoming K^- kicks one of the nucleons in deuteron in forward direction and loses its energy suitably to form $\Lambda(1405)$ with the other nucleon. Although a single scattering process also contributes to the $\Lambda(1405)$ production, for energetic incoming K^- with several hundreds MeV/c in the laboratory frame the contribution is small due to insufficient Fermi motion of nucleon in deuteron. In addition, thanks to the fact that strangeness is brought into the system by the incoming K^- , $\Lambda(1405)$ is formed selectively by the $\bar{K}N$ channel¹. This is a good advantage over $\Lambda(1405)$ productions induced by a nonstrange particle, in which strangeness has to be created in the reaction process and can be carried by the baryon producing $\Lambda(1405)$. In fact, there has been already an old bubble-chamber experiment observing $\Lambda(1405)$ in $K^-d \rightarrow \pi^+\Sigma^-n$ at K^- momenta between 686 and 844 MeV/c [23]. Although the statistics was not so high, the experiment found clearly that the $\Lambda(1405)$ spectrum has a peak at 1420 MeV. Forthcoming experiments in J-PARC with high-intensity kaon beam are expected for more detailed and precise information on the properties of $\Lambda(1405)$ [24]. Recently it has been suggested in Ref. [25] that the threshold effect of the $\bar{K}Nn$ in the $K^-d \rightarrow \pi\Sigma n$ reaction could distort the $\Lambda(1405)$ spectrum if the peak position would be close to the $\bar{K}N$ threshold. However, a clear $\Lambda(1405)$ peak was observed in the old bubble chamber experiment [23], and the $\Lambda(1405)$ peak will be located so well separatedly from the $\bar{K}N$ threshold that the threshold effect does not affect the spectrum shape. In addition, since the $\Sigma(1385)$ resonance is far from the $\bar{K}N$ threshold, this issue is irrelevant for the $\Sigma(1385)$ resonance.

In this paper, we apply this K^- -induced production off deuteron target also to the $\Sigma(1385)$ resonance, which has $J^P = 3/2^+$ and $I = 1$ and is also located below the $\bar{K}N$ threshold. The $\Sigma(1385)$ is understood well in quark model point of view; it is classified in flavor decuplet. Nevertheless, there are few theoretical discussion on $\Sigma(1385)$ formation in the $\bar{K}N$ channel. In addition, for precise determination of the $\Lambda(1405)$ properties from experiments, it is very important to understand contributions of $\Sigma(1385)$ in the $\Lambda(1405)$ production process, because the $\Lambda(1405)$ and $\Sigma(1385)$ resonances are located at very similar energy having tens MeV widths and their spectra overlap each other. This reaction gives also important informations on the subthreshold productions of $\Lambda(1405)$ and $\Sigma(1385)$, which will be significant in the strange few-body bound systems of $\bar{K}NN$ [26], $\bar{K}KN$ [27] and $\pi\Lambda N$ [28]. We also evaluate background contributions against $K^-d \rightarrow Y^*N$ by considering pion exchange contributions, in order to make further comparison with the experimental spectra observed in Ref. [23].

This paper is organized as follows. In Sec. 2 we explain our scheme to calculate the production cross sections for the $\Sigma(1385)$ as well as $\Lambda(1405)$. In Sec. 3 we show our numerical

¹ Formation of $\Lambda(1405)$ by the $\pi\Sigma$ channel would take place by multi-pion exchange between two baryons. However, multi-pion exchange processes are absolutely negligible for the resonance formation with in-flight K^- .

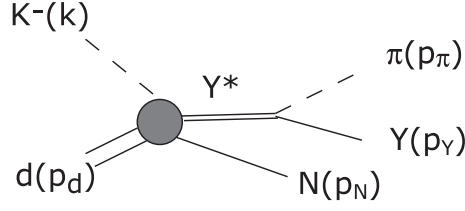


Fig. 1 Kinematics for the $K^-d \rightarrow \pi Y N$ reaction.

results of the calculations for the production cross sections. We also discuss nonresonant background contributions rather than $\Sigma(1385)$ and $\Lambda(1405)$ to the mass spectra in this section. Section 4 is devoted to the summary of this study.

2. Formulation

In this study we consider the $K^-d \rightarrow \pi^0 \Lambda n$, $(\pi\Sigma)^0 n$, $\pi^- \Lambda p$, and $(\pi\Sigma)^- p$ reactions so as to discuss the production of the hyperon resonances $\Sigma(1385)$ and $\Lambda(1405)$ initiated by the $\bar{K}N$ channel. The kinematical variables are given in Fig. 1. We discuss the kinematical aspects of the reactions in Sec. 2.1, and in the proceeding sections we discuss the dynamics of the reaction including the scattering amplitudes for K^-d reaction in Sec. 2.2 and the meson-baryon scattering amplitudes in Appendix.

2.1. Reaction kinematics

The reaction $K^-d \rightarrow \pi Y N$ requires five variables to completely fix the phase-space of the three-body final state [29]. In this study we are interested in the mass spectra of the πY systems, thus we choose as the five variables the πY invariant mass $M_{\pi Y}$, the solid angle of the final N in the total center-of-mass frame Ω_N , and the solid angle of the final π in the πY center-of-mass Ω_π^* . Then, the cross section of the reaction is calculated by,

$$d\sigma = \left(\frac{M_d M_Y M_N}{(2\pi)^4 4k_{\text{c.m.}} E_{\text{c.m.}}} \right) |\mathcal{T}|^2 |\mathbf{p}_N| |\mathbf{p}_\pi^*| dM_{\pi Y} d\cos\theta_N d\Omega_\pi^*, \quad (1)$$

where M_d , M_Y , and M_N are initial-state deuteron and final-state hyperon and nucleon masses in the reaction, respectively, $E_{\text{c.m.}}$ is the total center-of-mass energy, $k_{\text{c.m.}}$ is the K^- momentum in the total center-of-mass frame, θ_N is the scattering angle of N with respect to K^- in the total center-of-mass frame, and \mathcal{T} is the T -matrix of the reaction. In this form the azimuthal angle of the Ω_N is integrated.

Now let us pin down the reaction mechanism. Since we want to produce the hyperon resonances in the final state, the diagrams in which π and Y come from the same vertices are essential. Here, following Ref. [19] we evaluate the impulse and double-scattering amplitudes for the productions of the hyperon resonances.

First we consider the K^-d reaction with neutron emission in the final state. In this reaction the relevant diagrams are given in Fig. 2. Diagram 1 in Fig. 2 corresponds to the impulse process for the hyperon resonance production, whereas diagrams 2 and 3 are double scattering processes. We emphasize that the conservation of the strangeness in the strong interaction guarantees the production of hyperon resonances from the $\bar{K}N$ channel both in the impulse and the double scattering processes. The πY systems are fixed as charge zero ones, $\pi^0 \Lambda$, $\pi^+ \Sigma^-$, $\pi^- \Sigma^+$, and $\pi^0 \Sigma^0$. The $\pi^0 \Lambda$ ($\pi^0 \Sigma^0$) mass spectrum will be dominated by

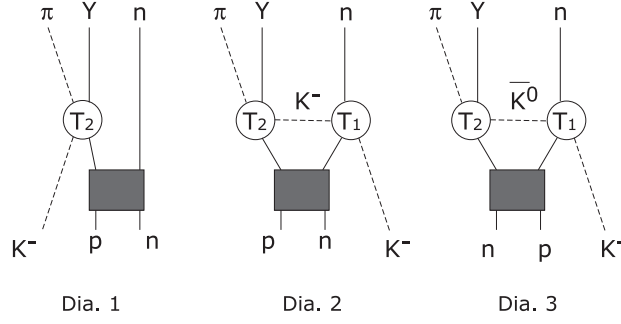


Fig. 2 Diagrams for the $K^-d \rightarrow \pi Y n$ reaction. In the diagrams T_1 and T_2 denote the scattering amplitudes for $K^-N \rightarrow \bar{K}n$ and $\bar{K}N \rightarrow \pi Y$, respectively.

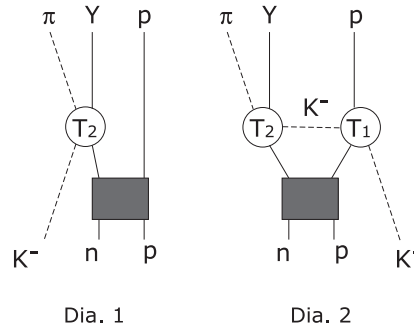


Fig. 3 Diagrams for the $K^-d \rightarrow \pi Y p$ reaction. In the diagrams T_1 and T_2 denote the scattering amplitudes for $K^-p \rightarrow K^-p$ and $K^-n \rightarrow \pi Y$, respectively.

the $\Sigma(1385)$ ($\Lambda(1405)$), since it is purely $I = 1$ (0) channel. The $\pi^+\Sigma^-$ and $\pi^-\Sigma^+$ mass spectra can contain $\Sigma(1385)$ in addition to $\Lambda(1405)$, since $\Sigma(1385)$ has the branching ratio 12% to the $\pi\Sigma$ channel.

Second we consider the K^-d reaction with proton emission in the final state. The relevant diagrams are given in Fig. 3. In this case we have only two diagrams so as to emit the final-state π and Y from same vertex; one is the impulse diagram and the other the double scattering diagram. The πY systems are $\pi^-\Lambda$, $\pi^-\Sigma^0$, and $\pi^0\Sigma^-$, and all of them contain only the $\Sigma^-(1385)$ contribution as hyperon resonances of interest.

Now that we have determined the reaction diagrams, all we have to do is the evaluation of the scattering amplitudes, which contains dynamics of the productions of the hyperon resonances.

2.2. K^-d Scattering amplitudes

In this section we formulate the scattering amplitudes of the K^-d reaction given in Figs. 2 and 3. These amplitudes are composed of $\bar{K}N \rightarrow \bar{K}N$ and πY amplitudes, kaon propagator, and deuteron wave function. We study both $\Sigma(1385)$ and $\Lambda(1405)$ in the reaction by including s - and p -wave contributions in the $\bar{K}N$ amplitudes. It is important that the p -wave contribution requires the nucleon spin component in the deuteron wave function, which is not needed in case of the $\Lambda(1405)$ production with the s -wave $\bar{K}N$ amplitudes [19].

First we formulate the amplitude of the impulse approximation given in Figs. 2(1) and 3(1). According to Ref. [19] and taking into account the spin component inside the deuteron, we can write the scattering amplitude for the impulse approximation as,

$$\mathcal{T}_{\pi Y n(1)}^a = T_{K^- p \rightarrow \pi Y}(M_{\pi Y}, \hat{p}_\pi \cdot \hat{k})(S^\dagger)^a \tilde{\varphi}(|\mathbf{p}_n - \frac{\mathbf{p}_d}{2}|) \quad , \quad (2)$$

$$\mathcal{T}_{\pi Y p(1)}^a = T_{K^- n \rightarrow \pi Y}(M_{\pi Y}, \hat{p}_\pi \cdot \hat{k})(S^\dagger)^a \tilde{\varphi}(|\mathbf{p}_p - \frac{\mathbf{p}_d}{2}|) \quad . \quad (3)$$

Here $T_{\bar{K}N \rightarrow MB}$ is the $\bar{K}N \rightarrow MB$ amplitude in the 2×2 matrix form, which compensates the Pauli spinor for baryons, and is function of center-of-mass energy $M_{\pi Y}$ and the angle $\hat{k} \cdot \hat{p}_\pi$ in meson-baryon center-of-mass frame, $(S^\dagger)^a = -i\sigma^2 \sigma^a / \sqrt{2}$ ($a = 1, 2, 3$) the spinor component for each nucleon inside the deuteron in 2×2 matrix form, and $\tilde{\varphi}(p)$ is the momentum representation of the deuteron wave function with momentum p , for which we neglect the d -wave component and use a parameterization of the s -wave component given by an analytic function [30] as,

$$\tilde{\varphi}(p) = \sum_{j=1}^{11} \frac{C_j}{p^2 + m_j} \quad , \quad (4)$$

with C_j and m_j determined in Ref. [31].

Second let us consider the double scattering amplitudes. According to Ref. [19] and taking into account the spin component inside the deuteron, the double scattering amplitudes are formulated as,

$$\begin{aligned} \mathcal{T}_{\pi Y n(2)}^a &= \int \frac{d^3 q}{(2\pi)^3} T_{K^- p \rightarrow \pi Y}(M_{\pi Y}, \hat{q} \cdot \hat{p}_\pi)(S^\dagger)^a T_{K^- n \rightarrow K^- n}^t(W, \hat{k} \cdot \hat{q}) \\ &\quad \times \frac{\tilde{\varphi}(|\mathbf{q} + \mathbf{p}_n - \mathbf{k} - \mathbf{p}_d/2|)}{q^2 - m_{K^-}^2 + i\epsilon} \quad , \end{aligned} \quad (5)$$

$$\begin{aligned} \mathcal{T}_{\pi Y n(3)}^a &= - \int \frac{d^3 q}{(2\pi)^3} T_{\bar{K}^0 n \rightarrow \pi Y}(M_{\pi Y}, \hat{q} \cdot \hat{p}_\pi)(S^\dagger)^a T_{K^- p \rightarrow \bar{K}^0 n}^t(W, \hat{k} \cdot \hat{q}) \\ &\quad \times \frac{\tilde{\varphi}(|\mathbf{q} + \mathbf{p}_n - \mathbf{k} - \mathbf{p}_d/2|)}{q^2 - m_{\bar{K}^0}^2 + i\epsilon} \quad , \end{aligned} \quad (6)$$

$$\begin{aligned} \mathcal{T}_{\pi Y p(2)}^a &= \int \frac{d^3 q}{(2\pi)^3} T_{K^- n \rightarrow \pi Y}(M_{\pi Y}, \hat{q} \cdot \hat{p}_\pi)(S^\dagger)^a T_{K^- p \rightarrow K^- p}^t(W, \hat{k} \cdot \hat{q}) \\ &\quad \times \frac{\tilde{\varphi}(|\mathbf{q} + \mathbf{p}_p - \mathbf{k} - \mathbf{p}_d/2|)}{q^2 - m_{K^-}^2 + i\epsilon} \quad , \end{aligned} \quad (7)$$

where q^0 and W is fixed as, $q^0 = k^0 + M_1 - p_N^0$ and $W = \sqrt{(M_1 + k^0)^2 - \mathbf{k}^2}$, with M_1 the first-scattered nucleon mass and p_N^0 the energy of the final-state nucleon. This prescription of q^0 takes account of the NN potential in deuteron nonperturbatively as suggested in the Watson formulation [21]. The superscript t denotes the transposition of the matrix in the spin space.

In our approach, the $\bar{K}N \rightarrow \bar{K}N$ and πY amplitudes are essential to the production of the hyperon resonances. For the meson-baryon amplitudes we apply the so-called chiral unitary approach [2–8]. In chiral unitary approach, $\Lambda(1405)$ is dynamically generated by the unitarized coupled-channel method based on chiral dynamics without explicit poles [14]. In contrast, $\Sigma(1385)$ can be included as an explicit pole in the p -wave kernel interactions in the

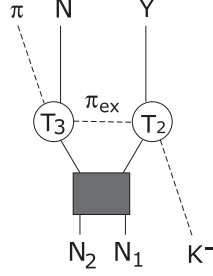


Fig. 4 Diagrams of the π meson exchange contribution. T_2 and T_3 denote the scattering amplitudes for $\bar{K}N \rightarrow \pi Y$ and $\pi N \rightarrow \pi N$, respectively.

coupled-channels [32]. The details of the description of the $\bar{K}N \rightarrow \bar{K}N$ and πY amplitudes for the $\Lambda(1405)$ and $\Sigma(1385)$ are given in Appendix A.

The chiral unitary amplitude has been calculated in the center of mass frame of the two-body meson baryon system. Since the deuteron wavefunction has been calculated in the rest frame of the deuteron, we calculate the $K^-d \rightarrow \pi YN$ amplitude in the lab frame, in which the target deuteron is at rest. Thus, we make a transformation of the amplitude obtained in the two-body center of mass frame to the baryon rest frame using the method shown in Appendix B. For the p -wave amplitude, we define the off-shell behavior by using a form factor

$$f_\Lambda(|\vec{q}|) = \frac{\Lambda^2}{\Lambda^2 + \vec{q}^2} \quad (8)$$

with $\Lambda = 630$ MeV, which has been used in the chiral unitary model for the s -wave.

The total amplitude for $K^-d \rightarrow \pi Yn$ and πYp is given by the coherent sum of the impulse and double scattering contributions as,

$$\mathcal{T}_{\pi Y n}^a = \mathcal{T}_{\pi Y n(1)}^a + \mathcal{T}_{\pi Y n(2)}^a + \mathcal{T}_{\pi Y n(3)}^a, \quad (9)$$

$$\mathcal{T}_{\pi Y p}^a = \mathcal{T}_{\pi Y p(1)}^a + \mathcal{T}_{\pi Y p(2)}^a, \quad (10)$$

respectively. Then, squared amplitude with spin-summed for final state and averaged in the initial state (deuteron) is given as,

$$|\mathcal{T}|^2 = \frac{1}{3} \sum_{a=1}^3 \text{tr}[\mathcal{T}^a (\mathcal{T}^a)^\dagger], \quad (11)$$

with taking the trace of the 2×2 spin space matrix by “tr”.

2.3. Estimation of the pion exchange contributions

It is instructive to estimate the pion exchange contribution to the production of the hyperon resonances, which mainly comes from the amplitudes without πY correlation in the final state. In the estimation of the pion exchange amplitude, we evaluate the diagrams given in Fig. 4. The particles, which are correlated to the pion exchange process, are listed in Table 1. They contain the $\pi N \rightarrow \pi N$ amplitudes, which do not appear in the usual diagrams for the production of hyperon resonances given in Figs. 2, 3. For the $\pi N \rightarrow \pi N$ amplitudes, we take empirically fitted one up to p -wave, including $\Delta(1232)$ resonance. We show the Dalitz plot in order to see the energy range of the πN amplitude. In Fig. 5, we have found the πN

Table 1 Possible exchange pions for the diagram shown in Fig. ??

Reaction	N_1	N_2	π_{ex}
$K^-d \rightarrow \pi^+\Sigma^-n$	p	n	π^+
	n	p	π^0
$K^-d \rightarrow \pi^-\Sigma^+n$	p	n	π^-
$K^-d \rightarrow \pi^0\Sigma^0n$	n	p	π^-
	p	n	π^0
$K^-d \rightarrow \pi^0\Lambda n$	n	p	π^-
	p	n	π^0
$K^-d \rightarrow \pi^-\Lambda p$	n	p	π^-
	p	n	π^0

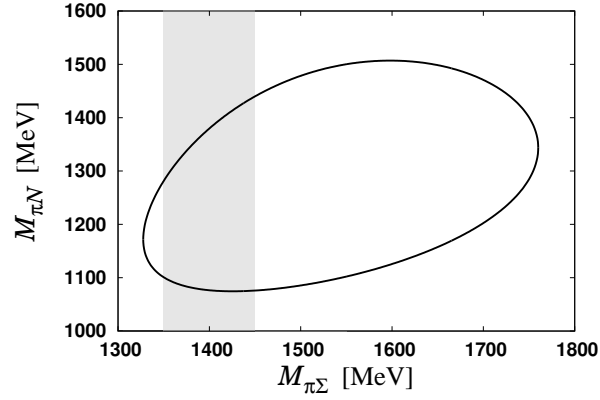


Fig. 5 Dalitz plot for $\pi^0\Sigma^0n$ final state with 800 MeV/c incident K^- momenta. Masked area shows the πY energy range (1350–1450 MeV) we considered in this work.

energy range, which is considered from $\Lambda(1405)$ and $\Sigma(1385)$ productions, includes $\Delta(1232)$ resonance. Therefore, the contribution of $\Delta(1232)$ production seems to be main smooth background from πN scattering in $\Lambda(1405)$ and $\Sigma(1385)$ productions.

3. Numerical results

In this section we show our numerical results for the production of hyperon resonances $\Sigma(1385)$ and $\Lambda(1405)$ in the K^-d reactions. Using Eq. (1), we can evaluate the differential cross section as,

$$\frac{d^2\sigma}{dM_{\pi Y}d\cos\theta_N} = \frac{M_d M_Y M_N}{(2\pi)^4 4k_{\text{c.m.}} E_{\text{c.m.}}} |\mathbf{p}_N| |\mathbf{p}_\pi^*| \int d\Omega_\pi^* |\mathcal{T}|^2, \quad (12)$$

with the $K^-d \rightarrow \pi Y N$ scattering amplitude \mathcal{T} which includes the pion exchange process. Then, integrating $\cos\theta_N$, one can obtain the πY mass spectrum,

$$\frac{d\sigma}{dM_{\pi Y}} = \frac{M_d M_Y M_N}{(2\pi)^4 4k_{\text{c.m.}} E_{\text{c.m.}}} |\mathbf{p}_N| |\mathbf{p}_\pi^*| \int_{-1}^1 d\cos\theta_N \int d\Omega_\pi^* |\mathcal{T}|^2 \quad (13)$$

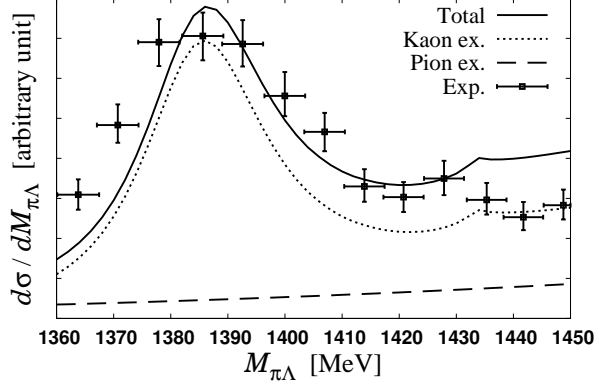


Fig. 6 $\pi^- \Lambda$ invariant-mass spectrum of the $K^- d \rightarrow \pi^- \Lambda p$ reaction in arbitrary units at 800 MeV/c incident K^- momentum. The solid line denotes the present calculation, and the dotted line and dashed line are the contribution from the kaon exchange and that from the pion exchange, respectively. Experimental data are taken from Ref. [23] at K^- momenta between 686 MeV/c and 844 MeV/c.

Further, integrating $M_{\pi Y}$ with appropriate range (M_{\min} , M_{\max}) for the hyperon resonances, the production cross section for the hyperon resonances is obtained as,

$$\sigma = \frac{M_d M_Y M_N}{(2\pi)^4 4k_{\text{c.m.}} E_{\text{c.m.}}} \int_{M_{\min}}^{M_{\max}} dM_{\pi Y} |\mathbf{p}_N| |\mathbf{p}_\pi^*| \int_{-1}^1 d\cos\theta_N \int d\Omega_\pi^* |\mathcal{T}|^2. \quad (14)$$

It is also interesting to calculate the angular dependence of the production by,

$$\frac{d\sigma}{d\cos\theta_N} = \frac{M_d M_Y M_N}{(2\pi)^4 4k_{\text{c.m.}} E_{\text{c.m.}}} \int_{M_{\min}}^{M_{\max}} dM_{\pi Y} |\mathbf{p}_N| |\mathbf{p}_\pi^*| \int d\Omega_\pi^* |\mathcal{T}|^2. \quad (15)$$

In this study we evaluate the $K^- d$ amplitudes in Figs. 2 and 3 by using chiral unitary approach for the description of the meson-baryon scattering amplitudes. In this approach $\Lambda(1405)$ is dynamically generated without introducing explicit poles in the s -wave, whereas $\Sigma(1385)$ is included as an explicit pole in the p -wave amplitude.

First we compare our results with experiments in Sec. 3.1. Next in Sec. 3.2 theoretical studies of the production of the hyperon resonances are given.

3.1. Production of hyperon resonances – comparison with experimental data

3.1.1. $\Sigma(1385)$ production. First of all, we show the results of the $\Sigma(1385)$ production and make a comparison with the experimental data [23]. For the $\Sigma(1385)$ production, it is better to see the $K^- d \rightarrow \pi^- \Lambda p$ reaction, in which $\Lambda(1405)$ does not contribute to the $\pi^- \Lambda$ mass spectrum. Here, we include the pion exchange contribution in addition to the kaon exchange contribution for the hyperon resonance production.

Using Eq. (13), we show the $\pi^- \Lambda$ mass spectrum in the $K^- d \rightarrow \pi^- \Lambda p$ reaction in Fig. 6, together with the experimental data [23], which includes the background contribution. Here the kaon momentum is fixed as 800 MeV/c in our calculation, whereas the range of the initiated kaon momentum is from 686 to 844 MeV/c in the experiment [23]. As seen in the figure, we can well reproduce the experimental mass spectrum with the $\Sigma(1385)$ peak around 1385 MeV of the $\pi^- \Lambda$ invariant mass.

Next, let us evaluate the cross section of the $\Sigma(1385)$ production by considering only the kaon exchange contribution. From the kaon exchange mass spectrum given in Fig. 6 (dotted line), we take the integration range $M_{\min} = 1370$ MeV and $M_{\max} = 1400$ MeV. Then, the cross section of the $\Sigma(1385)$ production is obtained as,

$$\sigma_{\Sigma^*} = \frac{1}{0.88} \int_{M_{\min}}^{M_{\max}} dM_{\pi^-\Lambda} \frac{d\sigma_{\text{F.G.}}}{dM_{\pi^-\Lambda}}, \quad (16)$$

where factor $1/0.88$ comes from the branching ratio of $\Sigma(1385) \rightarrow \pi\Lambda$, 88%. We obtain the $\Sigma(1385)$ production cross section as $179 \mu\text{b}$ with $800 \text{ MeV}/c$ incident K^- , whereas the experimental value observed in the $K^-d \rightarrow \pi^-\Lambda p$ reaction is reported to be $252 \pm 30 \mu\text{b}$ at $778 \text{ MeV}/c$ of the incident K^- momentum [23]. As one can see, our cross section is consistent with the experimental value. There is, however, small difference between our theoretical production cross section and the experimental one. This difference may come from the ways to subtract background contribution of the resonance. In ref. [23], the background contributions have been estimated by fitting the mass spectrum in a sum of Legendre polynomials together with a relativistic Breit-Wigner form for the resonance. In the theoretical side, we have estimated the production cross section by using the diagrams in which π^- and Λ are emitted from the same vertex and we have not subtracted the non-resonant background appearing in the $K^-n \rightarrow \pi^-\Lambda$ amplitude against the $\Sigma(1385)$, which is clearly seen above the 1400 MeV of the invariant mass $\pi^-\Lambda$. We also note that the value of the production cross section depends on the choice of the range of the invariant mass integration.

At last we should note that above the 1420 MeV of the $\pi^-\Lambda$ invariant mass the mass spectrum is not suppressed although this is a far above the $\Sigma(1385)$ energy region. This comes from $I = 1$ non-resonant background in the $\bar{K}N$ scattering, which can interfere to $\Lambda(1405)$.

3.1.2. $\Lambda(1405)$ production. Next we show the results of the $\Lambda(1405)$ production in the K^-d reaction. For the $\Lambda(1405)$ production we choose $K^-d \rightarrow \pi^+\Sigma^-n$ reaction and calculate the $\pi^+\Sigma^-$ mass spectrum. Here we note that $\pi^+\Sigma^-$ spectrum is contributed not only from $\Lambda(1405)$ but also from $\Sigma^0(1385)$, whose branching ratio to $\pi\Sigma$ is about 12%.

First, we show the $\pi^+\Sigma^-$ mass spectrum of the $K^-d \rightarrow \pi^+\Sigma^-n$ reaction in Fig. 7, together with the experimental data [23]. The background of the experiment has been assumed to be a sum of Legendre polynomials and is included into the mass spectrum. In the previous paper [19] the K^-d reaction with only s -wave meson-baryon amplitude has been calculated, whereas in this study we include both s - and p -wave meson-baryon amplitudes. In Fig. 7, we plot the full calculation with coherent sum of s - and p -wave contributions by the solid line, whereas the s - (p -) wave contribution in $\bar{K}N \rightarrow \pi^+\Sigma^-$ amplitude (T_2 in Figs. 2 and 3) is shown by the dashed (dotted) line. The $K^-N \rightarrow \bar{K}N$ amplitudes T_1 in Figs. 2 and 3 are fixed to be coherent sum of the s - and p -wave contributions in every case. As you can see from the figure, we reproduce well the experimentally observed mass spectrum of the reaction. We can see the $\Lambda(1405)$ peak appears at 1420 MeV in $\pi^+\Sigma^-$ invariant mass instead of nominal 1405 MeV as in Ref. [19], without contamination from $\Sigma(1385)$ nor p -wave background contribution. Furthermore, it is important that $\Sigma(1385)$ contribution appears as a shoulder around 1390 MeV $\pi^+\Sigma^-$ invariant mass, which may explain with the bump structure in the empirical data.

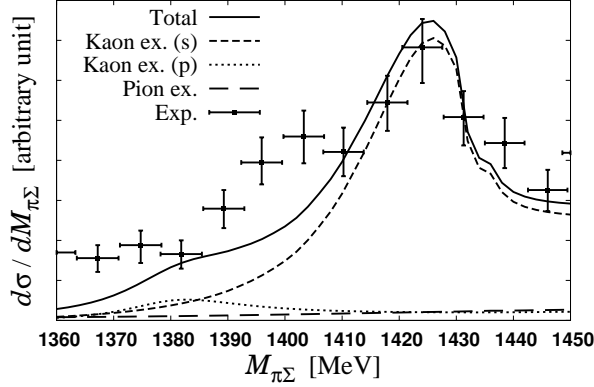


Fig. 7 $\pi^+\Sigma^-$ invariant-mass spectrum of the $K^-d \rightarrow \pi^+\Sigma^-n$ reaction in arbitrary units at 800 MeV/c incident K^- momentum. The solid line denotes the result of the full calculation with both s - and p -wave contributions, whereas the dashed (dotted) line denotes the contribution from the kaon exchange s - (p -) wave component in the $\bar{K}N \rightarrow \pi^+\Sigma^-$ amplitude. The dashed line corresponds to the result in Ref. [19]. The long-dashed line denotes the pion exchange contribution. Experimental data are taken from Ref. [23] at K^- momenta between 686 MeV/c and 844 MeV/c.

Next, let us consider the $\Lambda(1405)$ production cross section from the kaon exchange contribution, which is calculated by the formula,

$$\sigma_{\Lambda^*} = 3 \int_{M_{\min}}^{M_{\max}} dM_{\pi^+\Sigma^-} \frac{d\sigma_{\text{F.G}}}{dM_{\pi^+\Sigma^-}} \quad (17)$$

with the range $M_{\min} = 1400$ MeV and $M_{\max} = 1440$ MeV. The factor 3 comes from the branching ratio of $\Lambda(1405) \rightarrow \pi^+\Sigma^-$, 33%. The $\Lambda(1405)$ production cross section is consistent with the empirical value [23], as obtained previously in Ref. [19].

3.2. Production of hyperon resonances – theoretical studies

For the understanding of the production of the hyperon resonances in the K^-d reaction, it is important to investigate theoretically the production mechanism of the reaction. Therefore, we make theoretical studies of the K^-d reaction in this subsection.

3.2.1. $\pi\Sigma$ channel components. For the clarification of the $\Lambda(1405)$ properties, it is important to understand the behavior of the each $\pi\Sigma$ channel spectrum. Hence, we plot the $\pi^+\Sigma^-$, $\pi^-\Sigma^+$, and $\pi^0\Sigma^0$ mass spectra in the $K^-d \rightarrow (\pi\Sigma)^0n$ reaction in Fig. 8. Here the initial kaon momentum is fixed as 800 MeV/c.

From Fig. 8 one can see that the behavior of the $\pi\Sigma$ mass spectra is slightly different from each other. This is due to the interference between the $\Lambda(1405)$ contribution ($I = 0$) and the $I = 1$ non-resonant contribution. The significant non-resonant contribution with $I = 1$ around the $\Lambda(1405)$ energy can be seen in the $\pi^-\Lambda$ spectrum shown in Fig. 6. As a consequence of the interference, the $\pi^+\Sigma^-$ spectrum shows the largest contribution of the $\Lambda(1405)$ production and has the peak position at higher energy than the $\pi^-\Sigma^+$ spectrum, which are consistent with the results obtained in Ref. [19]. The interference between the

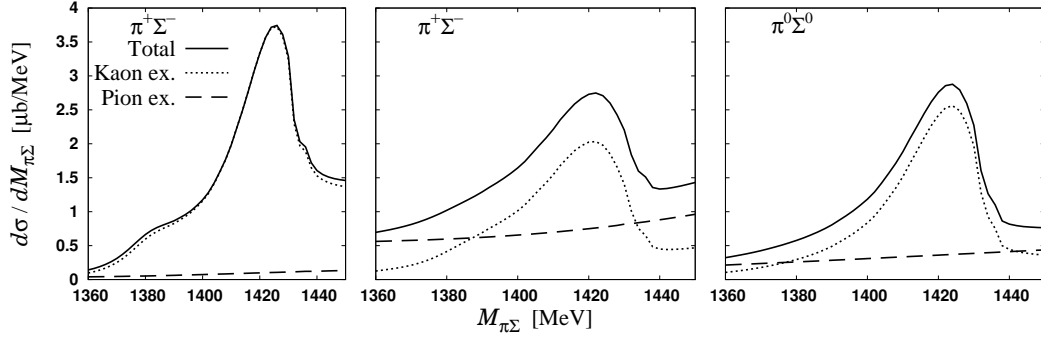


Fig. 8 $\pi\Sigma$ invariant-mass spectrum for different $\pi\Sigma$ states at 800 MeV/c incident K^- momentum.

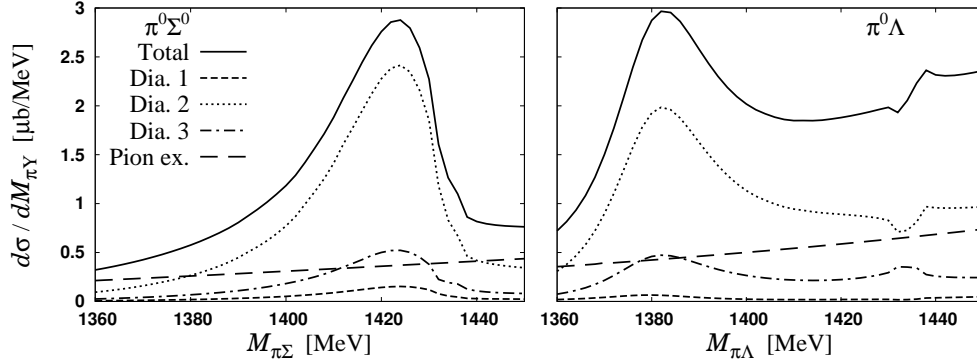


Fig. 9 $\pi^0\Sigma^0$ (left panel) and $\pi^0\Lambda$ (right panel) invariant-mass spectrum separately plotted in each diagram contribution. The incident K^- momentum is at 800 MeV/c. The solid line shows the kaon exchange contributions of three diagrams and the pion exchange diagrams. The dashed, dotted and dash-dotted line show the contribution from diagram 1, 2 and 3 as shown in Fig. 2, respectively. The long-dashed line shows the pion exchange contribution.

$\Lambda(1405)$ and $I = 1$ contributions has been, indeed, important in the photoproduction of $\Lambda(1405)$ [34–36]. Therefore, experimental data on the $\pi^\pm\Sigma^\mp$ spectrum will bring us further information of the $\Lambda(1405)$ structure.

We also note that the $\pi^0\Sigma^0$ spectrum does not show the $\Sigma(1385)$ contribution, because the $\pi^0\Sigma^0$ channel does not contain $I = 1$ component. Hence, it will be important to observe all the three $(\pi\Sigma)^0$ spectra in the K^-d reaction and compare them in the experiment for the understanding of the $\Lambda(1405)$ structure.

3.2.2. Diagram contributions. For the understanding of the K^-d reaction it is helpful to investigate each diagram contribution to the production of the hyperon resonances. Here we show the $\pi^0\Sigma^0$ and $\pi^0\Lambda$ invariant mass spectra separately plotted in each diagram contribution in Fig. 9. The incident kaon momentum is 800 MeV/c.

As you can see, both $\Lambda(1405)$ in the $\pi^0\Sigma^0$ spectrum and $\Sigma(1385)$ in the $\pi^0\Lambda$ spectrum show that diagram 1 (impulse contribution) in the reaction (Fig. 2) has quite small contribution, whereas diagram 2 in the reaction (Fig. 2) has the largest contribution. The reason that

diagram 1 corresponding to the impulse production of the hyperon resonances gives small contribution is that deuteron hardly has the high momentum component of the inside nucleons as discussed in Ref. [19]. Namely, in order to produce the hyperon resonances below the $\bar{K}N$ threshold, one needs to create an energetic nucleon in the final state of the $K^-d \rightarrow \pi Y N$ reaction. Such an energetic nucleon is, however, scarcely produced in the impulse process of the K^-d reaction, because large Fermi momentum of the nucleon is highly suppressed by the deuteron wave function due to the small binding energy. As a consequence, the impulse production of the hyperon resonances has quite small contribution.

Compared with the impulse process, the double scattering process (diagram 2 and 3) is kinematically favored. Namely in the double scattering process the transferred energy can be taken from the incident kaon so that the exchanged kaon has less energy than on-shell, which is favorable for the production of hyperon resonances below the $\bar{K}N$ threshold. Among the double scattering, since the $K^-n \rightarrow K^-n$ amplitude takes larger value than that of the $K^-p \rightarrow \bar{K}^0 n$ amplitude in the considering energy region, the diagram 2 has the largest contribution to both the $\Lambda(1405)$ and $\Sigma(1385)$ production (see also discussion in Ref. [19]).

3.2.3. Angular dependence of production. Now let us see the angular dependence of the production of the hyperon resonances. First of all, we show the double differential cross section $d^2\sigma/dM_{\pi\Sigma}d\cos\theta_n$ in the $K^-d \rightarrow \pi^+\Sigma^-n$ reaction in Fig. 10, in which the incident kaon momentum is fixed to be 800 MeV/c. In this reaction we can see the two peaks coming from two resonances, $\Sigma(1385)$ around 1385 MeV and $\Lambda(1405)$ around 1420 MeV, for $60^\circ \leq \theta_n \leq 150^\circ$.

As one can see, the $\Lambda(1405)$ peak has strong angular θ_n dependence. The $\Lambda(1405)$ peak takes its largest value at $\theta_n = 0$ (deg.), which corresponds the forward neutron emission in the total center-of-mass frame, and it becomes about 10 times smaller in the region $\theta_n \geq 60$ (deg.). The reason is as follows. The momentum transfer by the exchanged kaon becomes smaller in the double scattering process in the region $\theta_n \leq 60$ (deg.), because in this case the incident kaon kicks out neutron in the direction of incident kaon and gives most of its momentum simply to the neutron in the first step of the double scattering. This small momentum transfer makes the exchanged kaon close to be on the mass shell, in which the double scattering amplitude takes larger value. Hence, due to the kinematical reasons of the dominant double scattering (discussed in the previous section) and of the suitable momentum transfer, the $\Lambda(1405)$ peak has a large angular dependence and consequently backward $\Lambda(1405)$ production is dominated.

The $\Sigma(1385)$ peak, on the other hand, shows only small angular dependence in the $K^-d \rightarrow \pi^+\Sigma^-n$ reaction. This is caused by the p -wave nature of $\Sigma(1385)$ in the meson-baryon scattering. Namely, since the p -wave amplitude depends linearly on the transferred momentum, the $\Sigma(1385)$ cannot be much produced with the neutron forward angle, in which the momentum transfer becomes smaller (as discussed above). This momentum transfer becomes larger as the angle θ_n becomes larger, since the incident kaon has to kick out neutron in the opposite direction of the kaon momentum in the first step of the double scattering. Therefore, as a combination of p -wave nature of $\Sigma(1385)$ and suitable region of the momentum transfer in the process, $\Sigma(1385)$ production shows small angular dependence although in the middle θ_n region the production is not favored by the kinematics.

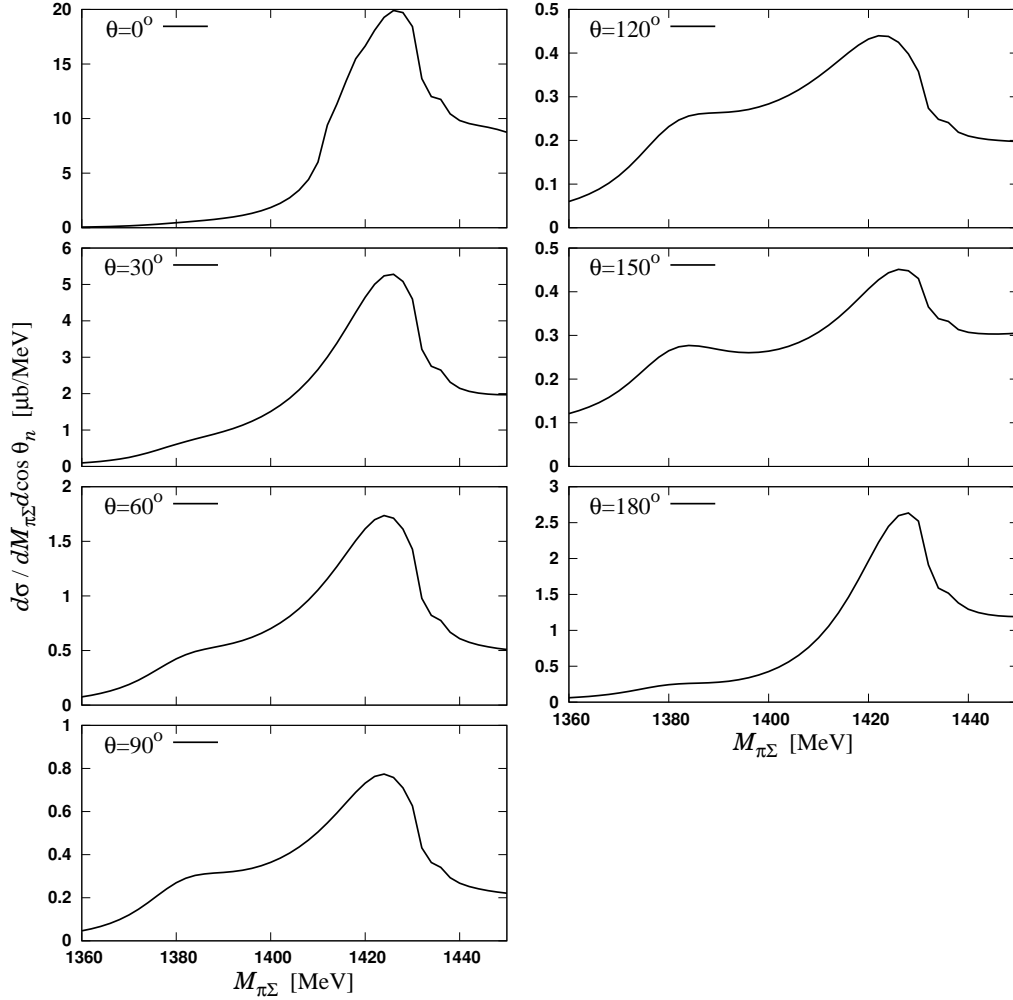


Fig. 10 Angular dependence of $\pi^+\Sigma^-$ invariant-mass spectrum at 800 MeV/c incident K^- momentum. The values of θ in the figure is in unit of degrees.

The angular dependence of the hyperon resonance production is clearly seen in the differential cross section $d\sigma/d\cos\theta_n$ with the integration range (M_{\min} , M_{\max}) given in Sec. 3.1. In Fig. 11, we plot the $d\sigma/d\cos\theta_n$ for the $\Lambda(1405)$ ($\Sigma(1385)$) production in the $K^-d \rightarrow \pi^0\Sigma^0n$ ($\pi^0\Lambda n$) reaction. From Fig. 11, we can see that the $\Lambda(1405)$ is produced dominantly in the forward neutron angle, whereas the $\Sigma(1385)$ production moderately depends on the neutron angle.

3.2.4. Missing mass spectrum. As we have seen in the previous sections, the $\Lambda(1405)$ peak appears at 1420 MeV instead of nominal 1405 MeV in the $\pi\Sigma$ invariant mass of the $K^-d \rightarrow \pi\Sigma n$ reaction thanks to the selective $\Lambda(1405)$ production by the $\bar{K}N$ channel. This fact implies that there is a possibility that the $\Sigma(1385)$ and $\Lambda(1405)$ peaks are seen separately in the $\pi\Sigma$ mass spectrum of the K^-d reaction, which are usually mixed with each other due to the similar peak energies. Here in order to investigate the behavior of the peak structures, we plot the missing mass spectrum of the reaction $K^-d \rightarrow nX$. In the energy region around 1400 MeV, the missing mass spectrum is expected to be dominated by the $(\pi Y)^0$ system.

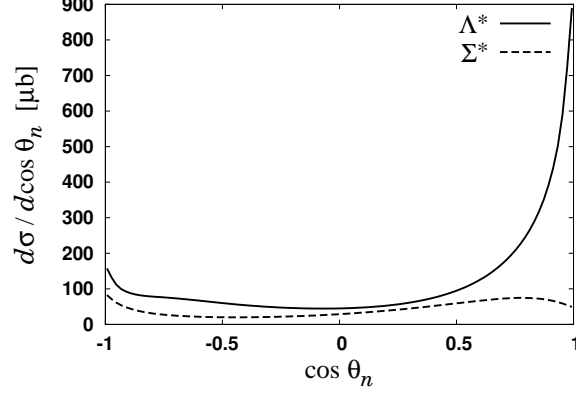


Fig. 11 Angular dependence of the $\Lambda(1405)$ and $\Sigma^0(1385)$ production cross sections in $K^-d \rightarrow \pi^0 \Sigma^0 n$ (for $\Lambda(1405)$) and $\pi^0 \Lambda n$ (for $\Sigma^0(1385)$) reactions.

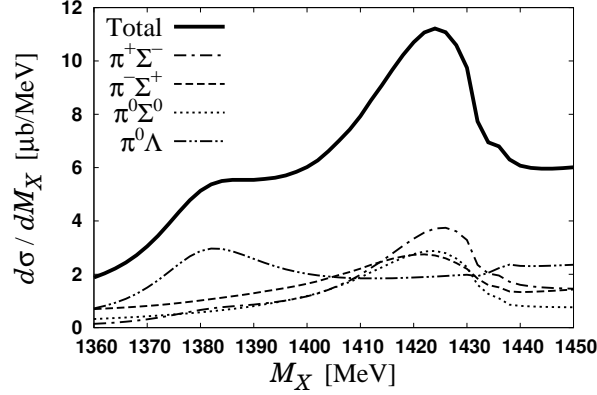


Fig. 12 Missing mass spectrum in $K^-d \rightarrow nX$ process at 800 MeV/ c incident K^- momentum. The solid, dashed, dashed-dotted, and dashed-double dotted lines are total, $\pi^-\Sigma^+$, $\pi^0\Sigma^0$, $\pi^+\Sigma^-$, and $\pi^0\Lambda$ contributions to X .

Hence, evaluating from the relevant diagrams shown in Figs. 2 and 3 and neglecting the amplitudes in which π and Y do not correlate to each other, which will make no structure in the missing mass spectrum, we can plot the missing mass spectrum in Fig. 12. As one can see, there appears the double-peak structure coming from $\Sigma(1385)$ (around 1385 MeV) and $\Lambda(1405)$ (around 1420 MeV). In the missing mass spectrum, the $\Sigma(1385)$ peak comes from $\pi^0\Lambda$ and the $\Lambda(1405)$ peak from $(\pi\Sigma)^0$ channel. The reason why we can separate the $\Sigma(1385)$ peak and the $\Lambda(1405)$ one is, as discussed above, we can produce $\Lambda(1405)$ from $\bar{K}N$ initial channel, pinning down the production process via conservation of the strangeness.

4. Summary

We have done the study of the $\Sigma(1385)$ and $\Lambda(1405)$ productions induced by K^- on a deuteron target by calculating the $K^-d \rightarrow \pi Y N$ reaction. We have taken into account both s - and p -wave contributions of the meson-baryon scatterings in the K^-d reaction, especially the contribution of the $\Sigma(1385)$ resonance is newly considered in this study. In the $K^-d \rightarrow \pi Y N$

reaction, the hyperon resonances are created selectively by the $\bar{K}N$ channel. Thanks to this fact, the higher pole state of $\Lambda(1405)$ is produced and the $\pi\Sigma$ spectrum has a peak at around 1420 MeV. This finding implies that the $\Lambda(1405)$ and $\Sigma(1385)$ could be seen separately in the missing mass spectrum of the emitted nucleon in the $K^-d \rightarrow nX$ reaction. We have found that invariant mass spectrum of πY is consistent with experimental data [23], both for $\Sigma(1385)$ and $\Lambda(1405)$ cases. We have investigated the angular dependence of the hyperon resonances and found that the $\Lambda(1405)$ production mainly takes place in the backward direction, while the $\Sigma(1385)$ production does not strongly depend on the angle of the emitted nucleon. We studied the production mechanisms of $\Sigma(1385)$ and $\Lambda(1405)$ from the theoretical side. We have also estimated the pion exchange contributions coming from diagrams in which π and Y is not correlated to each other and found that these contributions give smooth background and do not spoil the peak structure of the hyperon resonances.

Acknowledgment

This work was in part supported by the Grant-in-Aid for Scientific Research from MEXT and JSPS (Nos. 22740161, 24105706,), the collaboration agreement between the JSPS of Japan and the CSIC of Spain, and the Grant-in-Aid for the Global COE Program “The Next Generation of Physics, Spun from Universality and Emergence” from MEXT of Japan. This work is partly supported by DGICYT contract number FIS2006-03438. We acknowledge the support of the European Community-Research Infrastructure Integrating Activity ”Study of Strongly Interacting Matter” (acronym HadronPhysics2, Grant Agreement n. 227431) under the Seventh Framework Programme of EU. This work is part of the Yukawa International Program for Quark-Hadron Sciences (YIPQS).

References

- [1] R. H. Dalitz and S. F. Tuan, Phys. Rev. Lett. **2**, 425 (1959); Annals Phys. **10**, 307 (1960).
- [2] N. Kaiser, P. B. Siegel and W. Weise, Nucl. Phys. A **594**, 325 (1995) [arXiv:nucl-th/9505043].
- [3] E. Oset and A. Ramos, Nucl. Phys. A **635**, 99 (1998) [arXiv:nucl-th/9711022].
- [4] J. A. Oller and U. G. Meissner, Phys. Lett. B **500**, 263 (2001) [arXiv:hep-ph/0011146].
- [5] M. F. M. Lutz and E. E. Kolomeitsev, Nucl. Phys. A **700**, 193 (2002).
- [6] E. Oset, A. Ramos and C. Bennhold, Phys. Lett. B **527**, 99 (2002) [Erratum-ibid. B **530**, 260 (2002)] [arXiv:nucl-th/0109006].
- [7] T. Hyodo, S. I. Nam, D. Jido, and A. Hosaka, Phys. Rev. C **68**, 018201 (2003); Prog. Theor. Phys. **112**, 73 (2004).
- [8] D. Jido, J. A. Oller, E. Oset, A. Ramos and U. G. Meissner, Nucl. Phys. A **725**, 181 (2003) [arXiv:nucl-th/0303062].
- [9] B. Borasoy, R. Nissler and W. Weise, Eur. Phys. J. **A25**, 79 (2005).
- [10] B. Borasoy, U. -G. Meissner, R. Nissler, Phys. Rev. **C74**, 055201 (2006) [hep-ph/0606108].
- [11] T. Hyodo and D. Jido, Prog. Part. Nucl. Phys. **67**, 55 (2012) arXiv:1104.4474 [nucl-th].
- [12] Y. Ikeda, T. Hyodo and W. Weise, Phys. Lett. B **706**, 63 (2011) [arXiv:1109.3005 [nucl-th]].
- [13] Y. Ikeda, T. Hyodo and W. Weise, Nucl. Phys. A **881**, 98 (2012) [arXiv:1201.6549 [nucl-th]].
- [14] T. Hyodo, D. Jido and A. Hosaka, Phys. Rev. C **78**, 025203 (2008).
- [15] T. Hyodo, A. Hosaka, M. J. Vicente Vacas and E. Oset, Phys. Lett. B **593**, 75 (2004).
- [16] M. F. M. Lutz and M. Soyeur, Nucl. Phys. A **748**, 499 (2005).
- [17] V. K. Magas, E. Oset and A. Ramos, Phys. Rev. Lett. **95**, 052301 (2005).
- [18] L. S. Geng, E. Oset and M. Doring, Eur. Phys. J. **A32**, 201 (2007).
- [19] D. Jido, E. Oset and T. Sekihara, Eur. Phys. J. A **42**, 257 (2009) [arXiv:0904.3410 [nucl-th]].
- [20] D. Jido, E. Oset and T. Sekihara, Eur. Phys. J. A **47**, 42 (2011) [arXiv:1008.4423 [nucl-th]].
- [21] D. Jido, E. Oset and T. Sekihara, arXiv:1207.5350 [nucl-th].
- [22] J. Esmaili, Y. Akaishi and T. Yamazaki, Phys. Rev. C **83**, 055207 (2011) [arXiv:0909.2573 [nucl-th]].
- [23] O. Braun *et al.*, Nucl. Phys. B **129**, 1 (1977).
- [24] H. Noumi *et al.*, J-PARC proposal E31 “Spectroscopic study of hyperon resonances below $\bar{K}N$ threshold via the (K^-, n) reaction on Deuteron” (2009).
- [25] K. Miyagawa and J. Haidenbauer, Phys. Rev. C **85**, 065201 (2012).
- [26] T. Yamazaki and Y. Akaishi, Phys. Lett. **B535**, 70 (2002).
- [27] D. Jido and Y. Kanada-En’yo, Phys. Rev. **C78**, 035203 (2008).
- [28] A. Gal and H. Garcilazo, Phys. Rev. **D78**, 014013 (2008).
- [29] K. Nakamura *et al.* [Particle Data Group Collaboration], J. Phys. G **37**, 075021 (2010).
- [30] M. Lacombe, B. Loiseau, R. Vinh Mau, J. Cote, P. Pires and R. de Tourreil, Phys. Lett. B **101**, 139 (1981).
- [31] R. Machleidt, Phys. Rev. C **63**, 024001 (2001).
- [32] D. Jido, E. Oset and A. Ramos, Phys. Rev. C **66**, 055203 (2002) [arXiv:nucl-th/0208010].
- [33] S. Prakhov *et al.*, Phys. Rev. C **80**, 025204 (2009) [arXiv:0812.1888 [hep-ex]].
- [34] J. C. Nacher, E. Oset, H. Toki and A. Ramos, Phys. Lett. B **455**, 55 (1999) [arXiv:nucl-th/9812055].
- [35] M. Niiyama *et al.*, Phys. Rev. C **78**, 035202 (2008) [arXiv:0805.4051 [hep-ex]].
- [36] K. Moriya and R. Schumacher [CLAS Collaboration], Nucl. Phys. A **835**, 325 (2010) [arXiv:0911.2705 [nucl-ex]].
- [37] Center of Nuclear Study, World Wide Web site <http://gwdac.phys.gwu.edu/>
- [38] O. Braun, V. Hepp, H. Strobele, W. Wittek and P. Baillon, Nucl. Phys. B **203**, 349 (1982).

A. Chiral Unitary Model for $\Lambda(1405)$ and $\Sigma(1385)$

Let us briefly formulate the meson-baryon scattering amplitude in chiral unitary approach. First of all, in order to include the higher orbital angular momenta for the meson-baryon system, we expand the amplitude $T_{ji}(W, x)$ (i and j denote the initial and final meson-baryon channel, respectively, W the center-of-mass energy, and $x = \cos \theta$ with the scattering angle

θ in the center-of-mass frame) into the partial wave as,

$$T_{ji}(W, x) = F_{ji}(W, x)\delta_{s_j s_i} - iG_{ji}(W, x)(\hat{k}' \times \hat{k}) \cdot \boldsymbol{\sigma}_{s_j s_i}, \quad (\text{A1})$$

$$F_{ji}(W, x) = \sum_{l=0}^{\infty} \left[(l+1)f_+^{(l)}(W) + lf_-^{(l)}(W) \right]_{ji} P_l(x), \quad (\text{A2})$$

$$G_{ji}(W, x) = \sum_{l=1}^{\infty} \left[f_+^{(l)}(W) - f_-^{(l)}(W) \right]_{ji} P'_l(x). \quad (\text{A3})$$

Restricting the orbital angular momentum up to p -wave ($l = 1$), F and G can be written as,

$$F_{ji}(W, x) = f^{(s)}(W) + x(2f_+^{(p)}(W) + f_-^{(p)}(W)), \quad (\text{A4})$$

$$G_{ji}(W, x) = f_+^{(p)}(W) - f_-^{(p)}(W). \quad (\text{A5})$$

Then, we make unitarizations to the amplitudes in the algebraic equation as [32],

$$f^{(s)}(W) = (1 - f_{\text{tree}}^{(s)}g)^{-1}f_{\text{tree}}^{(s)}, \quad (\text{A6})$$

$$f_+^{(p)}(W) = (1 - f_{+ \text{tree}}^{(p)}g)^{-1}f_{+ \text{tree}}^{(p)}, \quad (\text{A7})$$

$$f_-^{(p)}(W) = (1 - f_{- \text{tree}}^{(p)}g)^{-1}f_{- \text{tree}}^{(p)}. \quad (\text{A8})$$

Here f_{tree} corresponds to the tree-level amplitude, giving the interaction kernel of the coupled-channel. In this study, we use the Weinberg-Tomozawa term to $f_{\text{tree}}^{(s)}$, same as in Ref. [19],

$$(f_{\text{tree}}^{(s)})_{ij} = -C_{ij} \frac{1}{4f^2} (2W - M_i - M_j) \sqrt{\frac{M_i + E_i}{2M_i}} \sqrt{\frac{M_j + E_j}{2M_j}}. \quad (\text{A9})$$

with the channel indices i and j , the baryon mass M , the meson decay constant $f = 1.123f_\pi$ ($f_\pi = 93$ MeV), and the baryon energy E . For the $f_{\pm \text{tree}}^{(p)}$, on the other hand, we choose the explicit Λ , Σ , and Σ^* Born terms, same as Eqs. (19)-(22) in Ref. [32]. The meson-baryon loop integral g in dimensional regularization are written as

$$\begin{aligned} g_l(W) &= i2M_l \int \frac{d^4q}{(2\pi)^4} \frac{1}{(P-q)^2 - M_l^2 + i\epsilon} \frac{1}{q^2 - m_l^2 + i\epsilon} \\ &= \frac{2M_l}{16\pi^2} \left\{ a_i(\mu) + \ln \frac{M_l^2}{\mu^2} + \frac{m_l^2 - M_l^2 + W^2}{2W^2} \ln \frac{m_l^2}{M_l^2} \right. \\ &\quad + \frac{\bar{q}_l}{W} [\ln(W^2 - (M_l^2 - m_l^2) + 2\bar{q}_l W) + \ln(W^2 + (M_l^2 - m_l^2) + 2\bar{q}_l W) \\ &\quad \left. - \ln(-W^2 + (M_l^2 - m_l^2) + 2\bar{q}_l W) - \ln(-W^2 - (M_l^2 - m_l^2) + 2\bar{q}_l W) \right\}, \end{aligned} \quad (\text{A10})$$

where m and M are the meson and baryon masses, respectively, μ is a regularization scale and a_i are subtraction constants in each of the isospin channels. Here we use same parameter as Refs. [19] and [32],

$$\begin{aligned} a_{\bar{K}N} &= -1.84, \quad a_{\pi\Sigma} = -2.00, \quad a_{\pi\Lambda} = -1.83 \\ a_{\eta\Lambda} &= -2.25, \quad a_{\eta\Sigma} = -2.38, \quad a_{K\Xi} = -2.67. \end{aligned} \quad (\text{A11})$$

Using the meson-baryon scattering amplitudes in the chiral unitary approach, we can calculate the cross sections of the $\bar{K}N$ to several channels. The cross sections are expressed

as,

$$\frac{d\sigma_{ij}}{d\Omega} = \frac{1}{16\pi^2} \frac{M_i M_j}{s} \frac{k'}{k} \left\{ |F_{ji}(W, x)|^2 + |G_{ji}(W, x)|^2 \sin^2 \theta \right\}, \quad (\text{A12})$$

with initial and final center-of-mass momenta k and k' .

B. Meson-baryon scattering amplitudes

In this appendix, we show a way to transform the amplitude obtained in the center of mass frame of the two body meson-baryon system to the amplitude in the baryon rest frame. The idea is that we first obtain the invariant amplitude from the cm amplitude. Next we make the transformation of the invariant amplitude to the baryon rest frame.

B.1. Invariant amplitude of meson-baryon scattering

The Lorentz invariant scattering amplitude of meson-baryon can be written in general in terms of two Lorentz invariant functions, A and B :

$$T = \bar{u}(p_2) [A(s, t) + \gamma \cdot K B(s, t)] u(p_1) \quad (\text{B1})$$

where p_1 and p_2 are the initial and final baryon momenta, respectively, the four-vector K is defined by $K = \frac{1}{2}(k_1 + k_2)$ with the initial and final meson momenta k_1 and k_2 , and the Mandelstam variables s and t are given by $s = (p_1 + k_1)^2$ and $t = (k_1 - k_2)^2$.

B.2. Scattering amplitudes in the c.m. frame

In the c.m. frame, the scattering amplitudes are written as

$$T(W, x) = F(W, x) - iG(W, x) (\hat{k}_2 \times \hat{k}_1) \times \vec{\sigma} \quad (\text{B2})$$

with the partial wave decomposition

$$F(W, x) = \sum_{\ell=0}^{\infty} [(\ell+1)f_{\ell+}(W) + \ell f_{\ell-}(W)] P_{\ell}(x) \quad (\text{B3})$$

$$G(W, x) = \sum_{\ell=1}^{\infty} [f_{\ell+}(W) - f_{\ell-}(W)] P'_{\ell}(x) \quad (\text{B4})$$

where $W = \sqrt{s}$ is the c.m. energy and $x = \cos \theta$ with the scattering angle θ in c.m. frame. The relation between (A, B) and (F, G) is given by

$$A = \frac{1}{2W} \left[\left(W + \frac{M_1 + M_2}{2} \right) \frac{F + xG}{a_1 a_2} + \left(W - \frac{M_1 + M_2}{2} \right) \frac{G}{b_1 b_2} \right] \quad (\text{B5})$$

$$B = \frac{1}{2W} \left[\frac{F + xG}{a_1 a_2} - \frac{G}{b_1 b_2} \right] \quad (\text{B6})$$

where $a = \sqrt{(E + M)/(2M)}$ and $b = \sqrt{(E - M)/(2M)}$ with the c.m. baryon energy E and baryon mass M .

B.3. Scattering amplitudes in the baryon rest frame

Let us consider the initial baryon at rest. The amplitude in this frame is given by

$$T = F'(W, x') - iG'(W, x') (\hat{k}'_2 \times \hat{k}'_1) \cdot \vec{\sigma} \quad (\text{B7})$$

where x' is the angle between \vec{k}'_1 and \vec{k}'_2 .

The baryon rest frame amplitudes, F' and G' , can be written in terms of the Lorentz invariant amplitudes, A and B , as

$$F'(W, x') = a'_2 \left[A(s, t) + \frac{1}{2} \left(\omega'_1 + \omega'_2 + \frac{|\vec{k}'_2|^2 - |\vec{k}'_1|^2}{E'_2 + M_2} \right) B(s, t) \right] \quad (\text{B8})$$

$$G'(W, x') = -a'_2 \frac{|\vec{k}'_1| |\vec{k}'_2|}{E'_2 + M_2} B(s, t) \quad (\text{B9})$$

where $a'_2 = \sqrt{(E'_2 + M_2)/(2M_2)}$ with the final baryon energy E'_2 in the initial baryon rest frame and the final baryon mass M_2 .

The kinematical variables are expressed in terms of W and $\cos \theta'$ as

$$|\vec{k}'_1| = \frac{W |\vec{k}_1|}{M_1} \quad (\text{B10})$$

$$\omega'_1 = \gamma W - M_1 \quad (\text{B11})$$

$$\omega'_2 = \frac{\omega_2 + \beta \cos \theta' \sqrt{\omega_2^2 - \gamma^2 m_2^2 (1 - \beta^2 \cos^2 \theta')}}{\gamma (1 - \beta^2 \cos^2 \theta')} \quad (\text{B12})$$

$$|\vec{k}'_2| = \frac{\beta \cos \theta' \omega_2 + \sqrt{\omega_2^2 - \gamma^2 m_2^2 (1 - \beta^2 \cos^2 \theta')}}{\gamma (1 - \beta^2 \cos^2 \theta')} \quad (\text{B13})$$

Substituting Eqs.(B5) and (B6) to Eqs.(B8) and (B9), we obtain

$$F'(W, x') = \frac{a'_2}{4W} \left[\left(2W + \omega'_1 + \omega'_2 + M_1 + M_2 + \frac{|\vec{k}'_2|^2 - |\vec{k}'_1|^2}{E'_2 + M_2} \right) \frac{F(W, x) + xG(W, x)}{a_1 a_2} + \left(2W - \omega'_1 - \omega'_2 - M_1 - M_2 - \frac{|\vec{k}'_2|^2 - |\vec{k}'_1|^2}{E'_2 + M_2} \right) \frac{G(W, x)}{b_1 b_2} \right] \quad (\text{B14})$$

$$G'(W, x') = -\frac{a'_2}{2W} \frac{|\vec{k}'_1| |\vec{k}'_2|}{E'_2 + M_2} \left[\frac{F(W, x) + xG(W, x)}{a_1 a_2} - \frac{G(W, x)}{b_1 b_2} \right] \quad (\text{B15})$$

where $x = \cos \theta$ and $x' = \cos \theta'$ with the angles between the mesons in the c.m. and baryon rest frames, respectively. These are related by the boost transformation:

$$\cos \theta = \frac{\gamma}{|\vec{k}_2|} (-\beta \omega'_2 + |\vec{k}'_2| \cos \theta') = \eta + \xi x' \quad (\text{B16})$$

where $\beta = |\vec{p}_1|/E_1$ and $\gamma = (1 - \beta^2)^{-1/2}$.

The amplitudes $F'(W, x')$ and $G'(W, x')$ can be decomposed by partial wave in Lab. frame.

$$F'(W, x') = \sum_{\ell=0}^{\infty} F'^{(\ell)} P_{\ell}(x') = \sum_{\ell=0}^{\infty} [(\ell+1)f'_{\ell+}(W) + \ell f'_{\ell-}(W)] P_{\ell}(x') \quad (\text{B17})$$

$$G'(W, x') = \sum_{\ell=1}^{\infty} G'^{(\ell)} P_{\ell}(x') = \sum_{\ell=1}^{\infty} [f'_{\ell+}(W) - f'_{\ell-}(W)] P_{\ell}(x') \quad (\text{B18})$$

where

$$F'^{(\ell)}(W) = \frac{2\ell+1}{2} \int_{-1}^1 dx' F'(W, x') P_{\ell}(x') \quad (\text{B19})$$

$$G'^{(\ell)}(W) = \frac{2\ell+1}{2\ell(\ell+1)} \int_{-1}^1 dx' (1-x'^2) G'(W, x') P'_{\ell}(x') \quad (\text{B20})$$

Here we have used

$$\int_{-1}^1 dx P_\ell(x) P_k(x) = \frac{2}{2\ell+1} \delta_{\ell k} \quad (\text{B21})$$

$$\int_{-1}^1 dx (1-x^2) P'_\ell(x) P'_k(x) = \int_{-1}^1 dx P_\ell^1(x) P_k^1(x) = \frac{2}{2\ell+1} \frac{(\ell+1)!}{(\ell-1)!} \delta_{\ell k}. \quad (\text{B22})$$